Journal for ImmunoTherapy of Cancer

Mitochondria-targeted photodynamic therapy triggers GSDME-mediated pyroptosis and sensitizes anti-PD-1 therapy in colorectal cancer

Yun Zhou,[1,2,3] Wenyao Zhang,[2] Boda Wang,[2] Pei Wang,[2] Danxiu Li,[4] Tianyu Cao,[2] Dawei Zhang,[5] Hua Han,[6] Mingfeng Bai,[7] Xin Wang,[1] Xiaodi Zhao,[2] Yuanyuan Lu [2]

To cite: Zhou Y, Zhang W, Wang B, *et al*. Mitochondria-targeted photodynamic therapy triggers GSDME-mediated pyroptosis and sensitizes anti-PD-1 therapy in colorectal cancer. *Journal for ImmunoTherapy of Cancer* 2024;**12**:e008054. doi:10.1136/jitc-2023-008054

► Additional supplemental material is published online only. To view, please visit the journal online (https://doi.org/10.1136/jitc-2023-008054).

YZ and WZ contributed equally.

Accepted 11 February 2024

For numbered affiliations see end of article.

Correspondence to
Dr Yuanyuan Lu;
luyuandreamer@aliyun.com

Dr Xin Wang;
wangx@fmmu.edu.cn

Dr Xiaodi Zhao;
leedyzhao@fmmu.edu.cn

ABSTRACT

Background The effectiveness of immune checkpoint inhibitors in colorectal cancer (CRC) is limited due to the low tumor neoantigen load and low immune infiltration in most microsatellite-stable (MSS) tumors. This study aimed to develop a mitochondria-targeted photodynamic therapy (PDT) approach to provoke host antitumor immunity of MSS-CRC and elucidate the underlying molecular mechanisms.

Methods The role and mechanism of mitochondria-targeted PDT in inhibiting CRC progression and inducing pyroptosis were evaluated both in vitro and in vivo. The immune effects of PDT sensitization on PD-1 blockade were also assessed in CT26 and 4T1 tumor-bearing mouse models.

Results Here, we report that PDT using IR700DX-6T, a photosensitizer targeting the mitochondrial translocation protein, may trigger an antitumor immune response initiated by pyroptosis in CRC. Mechanistically, IR700DX-6T-PDT produced reactive oxygen species on light irradiation and promoted downstream p38 phosphorylation and active caspase3 (CASP3)-mediated cleavage of gasdermin E (GSDME), subsequently inducing pyroptosis. Furthermore, IR700DX-6T-PDT enhanced the sensitivity of MSS-CRC cells to PD-1 blockade. Decitabine, a demethylation drug used to treat hematologic neoplasms, disrupted the abnormal methylation pattern of GSDME in tumor cells, enhanced the efficacy of IR700DX-6T-PDT, and elicited a potent antitumor immune response in combination with PD-1 blockade and IR700DX-6T-PDT.

Conclusion Our work provides clear a understanding of immunogenic cell death triggered by mitochondria-targeted PDT, offering a new approach for enhancing the efficacy of PD-1 blockade in CRC.

WHAT IS ALREADY KNOWN ON THIS TOPIC

⇒ Photodynamic therapy (PDT) using the translocation protein (TSPO)-targeted photosensitizer, IR700DX-6T, inhibited tumor progression in breast cancer, induced immunogenic cell death and activated anti-tumor immune responses.

WHAT THIS STUDY ADDS

⇒ In this study, we demonstrated that TSPO-targeted PDT inhibited the progression of colorectal cancer (CRC) in vitro and in vivo, triggered pyroptosis through the reactive oxygen species/p38/CASP3/gasdermin E (GSDME) axis, and enhanced anti-PD-1 antibody efficacy in microsatellite-stable (MSS) CRC. Moreover, decitabine, a classic methyltransferase inhibitor, increased GSDME expression through demethylation and induced dramatic tumor shrinkage and immune cell infiltration when used in combination with PDT and anti-PD-1 antibody in tumors with low endogenous GSDME expression.

HOW THIS STUDY MIGHT AFFECT RESEARCH, PRACTICE OR POLICY

⇒ TSPO-targeted PDT is a potential new therapeutic strategy for the treatment of MSS-CRC.

BACKGROUND

Colorectal cancer (CRC) is increasingly recognized as a highly prevalent form of malignancy globally, with an increasing incidence among Asians similar to that in Europe and the USA.[1 2] Most patients with CRC exhibit mismatch repair proficient (pMMR) or microsatellite stability (MSS), which results in limited responses to immune checkpoint inhibitors (ICIs) due to deficiency of mutated tumor antigens.[3 4]

With its advantages of specific targeting, spatiotemporal controllability, and extremely low invasiveness, photodynamic therapy (PDT) shows great promise in treating various malignant tumors.[5] PDT is achieved by excitation with a specific wavelength of light to generate reactive oxygen species (ROS), particularly singlet oxygen, which initiates the photochemical response, activating signal pathways and inducing irreversible cell death.[6] To address limitations such as insufficient luminous flux, PDT has been combined with RNA interference, chemotherapy,

photothermal therapy, and immunotherapy to achieve promising therapeutic effects.[7] The 18 kDa transporter protein (TSPO), a transmembrane protein located in the outer membrane of mitochondria, is related to mitochondrial metabolism, immune regulation and other cellular processes.[8] Its expression is particularly high in CRC, breast cancer, glioblastoma, and some other types of cancer.[9] In our previous study, we demonstrated the efficacy of IR700DX-6T as a TSPO-targeted photosensitizer in regressing breast cancer; however, the type of cell death and underlying molecular mechanisms remain unclear.[10]

Pyroptosis is a newly disclosed programmed cell death pathway. Gasdermin family proteins act as key executors of pyroptosis by inducing membrane permeabilization and releasing cytoplasmic contents through caspase-mediated cleavage.[11 12] In addition to suppressing cellular proliferation, invasion, and metastasis, pyroptosis can elicit immunogenic cell death (ICD), thereby enhancing tumor cell immunogenicity and promoting immune cell infiltration.[13 14] However, most tumor cells exhibit limited gasdermin E (GSDME) expression due to abnormal methylation-mediated silencing.[15] Therefore, it is crucial to explore innovative approaches for eliciting effective pyroptosis and immune response in tumors.

Here, we demonstrated that IR700DX-6T-PDT effectively inhibited CRC proliferation both in vitro and in vivo. IR700DX-6T-PDT induced pyroptosis, p38 phosphorylation, and caspase3 (CASP3)-dependent cleavage of GSDME. In cell lines with minimal GSDME expression due to promoter methylation, IR700DX-6T-PDT exhibited low efficacy. Decitabine, a methyltransferase inhibitor, reversed GSDME silencing by demethylating GSDME and promoted the efficacy of IR700DX-6T-PDT. Remarkably, the combination of decitabine, IR700DX-6T-PDT and an anti-PD-1 antibody greatly overcame the immunosuppressive environment and resulted in dramatic tumor shrinkage, thus providing a promising strategy for improving the efficacy of ICIs. Our findings shed new light on the mechanism of IR700DX-6T-PDT-induced tumor cell death and provided a novel combinational strategy for the treatment of "cold" tumors.

METHODS

Cell culture

Human CRC cell lines (HCT116, SW620, HCT15, DLD-1, LS174T, SW480, SW1463, RKO, HCT8, and Caco-2), a murine colon adenocarcinoma cell line (CT26), and a murine breast cancer cell line (4T1) were obtained from the American Type Culture Collection. DiFi and KM12SM cells were gifted by the Coffey laboratory (Vanderbilt University Medical Center). Human normal epithelial cells line (NCM460) was obtained from the INCELL. The CT26 cell line was stably transfected with Firefly luciferase (CT26-fLuc) following a pre-established protocol.[16] All cells were preserved at the State Key Laboratory of Holistic Integrative Management of Gastrointestinal Cancers (Xi'an, China). Cells were cultured in DMEM medium (Gibco, Carlsbad, California, USA), supplemented with 10% fetal bovine serum (FBS, Gibco), 1% antibiotics, nonessential amino acids and glutamine (Gibco) in a 5% CO_2 incubator at 37°C.

In vitro PDT

The cells were seeded in 96-well plates, protected from light, and the cell adhesion process was monitored. After cell adhesion, the medium in the well was discarded and replaced with a fresh medium containing different concentrations of IR700DX-6T (0.125, 0.25, 0.5, 1, and 2 µM) or DMSO to study photosensitizer concentration-dependent PDT effect. After 16 hours, cells were washed with fresh medium to remove the unbound photosensitizers. The 96-well plates were irradiated with an LED light (L690-66-60, Marubeni America, New York, New York, USA) at the wavelength of 670–710 nm for 27 J/cm^2 as previously described.[10 17] To study light dose-dependent PDT effect, the cells were incubated with 1 µM IR700DX-6T for 16 hours, and then irradiated at different light doses (4.5, 9, 18, and 27 J/cm^2). After light irradiation for 16 hours, the CCK8 reagent (GK10001, GLPBIO) was added to each well of the 96-well plates and cells were incubated at 37°C for 2 hours. The absorbance was read at 450 nm using a Thermo Fisher Scientific Varioskan Flash multimode reader (Thermo Fisher Scientific, Carlsbad, California, USA).

Hoechst 33342/propidium iodide staining

CT26 and HCT116 cells were seeded into 12-well plates and treated with 1 µM IR700DX-6T for 16 hours. The light dose applied to treat CT26 and HCT116 cells were 18 and 27 J/cm^2, respectively. After the indicated treatment, the apoptosis and necrosis assay kit (C1056, Beyotime) was used to stain the cells, and the propidium iodide (PI)-positive cells were observed under an inverted fluorescence microscope (Olympus 1×83, Tokyo, Japan).

Cell death detection with flow cytometry

IR700DX-6T-PDT-induced cell death was detected using an Annexin V-FITC apoptosis detection kit (C1062L, Beyotime), according to the manufacturer's protocol. The cell culture medium was collected at specified times, and adherent cells were washed with phosphate buffered saline (PBS). When the cells were digested with trypsin without EDTA, the cell culture medium was added. Cells were then gently aspirated, collected, and washed with PBS. After precipitation, the cells were resuspended in Annexin V-FITC binding solution and stained with 5 µL of Annexin V-FITC and 10 µL of PI staining solution. Cells were stained at room temperature (RT) in the absence of light for 15 min and immediately analyzed via flow cytometry (Sony SA3800, Tokyo, Japan). All data were analyzed using FlowJo (Tree Star, Ashland, Oregon, USA).

Lactate dehydrogenase release assay

Lactate dehydrogenase (LDH) was measured in the supernatant of cell culture in order to determine

pyroptosis. The cell was pretreated with Ac-DEVD-CHO (100 µM, HY-P1001, MedChemExpress, MCE), N-acetyl-L-cysteine (NAC; 5 mM, V900429, Sigma-Aldrich), p38 inhibitor SB202190 (10 µM, HY-10295, MCE) or without any of the above, for 4 hours, before PDT was carried out. LDH activity was measured using an LDH release assay kit (C0017, Beyotime) according to the manufacturer's protocol. The absorbance was measured at 490 nm.

ROS and mitochondrial ROS measurement

DCFH-DA (S0033M, Beyotime) and MitoSox Red dye (M36008, Invitrogen) were used to measure the total and mitochondria ROS, respectively, according to the manufacturer's protocol. Cells were stained with 10 µM DCFH-DA or 5 µM MitoSox Red dye for 30 min in the dark at 37°C. Fluorescence intensity was measured using flow cytometry (Sony SA3800).

Small interfering RNA transfection

Small interfering RNA (siRNA) targeting GSDME was designed and synthesized by Tsingke (Beijing, China). siRNA transfection was performed using Lipofectamine RNAiMAX Transfection Reagent (13778030, Thermo Fisher Scientific), following the manufacturer's instructions. RNA and proteins were extracted at 48 hours and 72 hours after transient transfection, respectively. The siRNA sequences were listed in online supplemental table 1.

RNA extraction and RT-qPCR

Total RNA was extracted from cells using an RNA purification kit (K0731, Thermo Fisher Scientific). The Prime Script RT Reagent Kit (RR036B, TaKaRa) was used for the reverse transcription of RNA into cDNA. qPCR was performed using a SYBR Premix Ex Taq Kit (11 199ES03, Yeasen) on a CFX96 Real-Time PCR Detection System (Bio-Rad, Hercules, California, USA). PCR primers are listed in online supplemental table 2.

Protein extraction and Western blot

Treated cell sample proteins were collected using RIPA buffer containing a protease inhibitor (P8340, Sigma-Aldrich) and phosphatase inhibitor (P0044, Sigma-Aldrich). The cell lysates were quantified, combined with SDS loading buffer and subjected to boiled for 10 min in order to be prepared for Western blot analysis following the standard protocol. The following antibodies were used: DFNA5/GSDME (ab215191) and GSDMD (ab219800, ab210070) were purchased from Abcam. CASP3 (#9662), cleaved-CASP3 (#9661), JNK (#9252), p-JNK (#4668), p38 (#8690), p-p38 (#4511), MEK (#9126), p-MEK (#9154), ERK (#4695), p-ERK (#4370), GAPDH (#5174), and secondary antibodies (#7074, #7076) were obtained from Cell Signaling Technology. ECL reagent (4AW011, 4A Biotech) was used on a Molecular Imager ChemiDox XRS$^+$ Imaging System with Image Lab software (Bio-Rad) to visualize blotted bands.

In vivo animal experiments

For in vivo experiments, female BALB/c mice or BALB/c (nu/nu) nude mice aged 6–8 weeks were obtained from the Experimental Animal Center of the Air Force Medical University (Xi'an, China) and raised in an SPF-grade room with a 12-hours light/12-hour dark cycle and fed a standard rat diet.

To establish a CT26 subcutaneous tumor model, we inoculated CT26-fLuc tumor cells (5×10^5) subcutaneously into the flank of mice. Tumor-bearing mice were randomly divided into four groups (n=5): PBS, anti-PD-1, IR700DX-6T+Light, and IR700DX-6T+Light with anti-PD-1. The IR700DX-6T+Light and IR700DX-6T+Light with anti-PD-1 groups were intravenous injected with 7.5 nM of IR700DX-6T in 100 µL of PBS through the tail vein on day 1. PDT was performed in vivo, as previously reported.[10] Two hours after the injection of the photosensitizer, the mice were anesthetized with a 2% (v/v) isoflurane/oxygen mixture. The tumors were then exposed to LED light at a wavelength of 670–710 nm (peak at 690 nm) with the light dose of 18 J/cm^2 administered at 30 mW/cm^2. After 24 hours of irradiation, the mice were initially intraperitoneally injected with 100 µg of anti-PD-1 antibody (clone: RMP1-14, BioXcell) and subsequently received injections every 3 days. The mice were treated with anti-PD-1 antibody four times. Measurements of mouse tumor size, weight, and bioluminescence imaging (BLI) were recorded regularly. Tumor volumes were measured every 3 days using vernier calipers and calculated as follows: (length×width^2)/2. On completion of the experiment, the mice were sacrificed according to institutional ethical guidelines.

To investigate the effect of decitabine combined with IR700DX-6T+Light and anti-PD-1, female BALB/c mice were subcutaneously injected with 4T-1 cells (5×10^5 cells per mouse). The mice were randomly divided into six groups (n=5): PBS, decitabine, decitabine+anti-PD-1, IR700DX-6T+Light, IR700DX-6T+Light+decitabine, and IR700DX-6T+Light+decitabine+anti-PD-1. Decitabine (80 µM, HY-A0004, MCE) was dosed for 3 days, and IR700DX-6T+Light (light dose of 18 J/cm^2) was performed soon after. Anti-PD-1 antibody was injected intraperitoneally on days 4, 7, 10, and 13 after cell injection, followed by twice-weekly injections.

Flow cytometry assay

After the treatment, the tumor was stripped and cut into a slurry using scissors. We used a digestive solution (1640 medium containing 2% FBS, 1 mg/mL collagenase IV (LS004188, Worthington Biochemical), and 200 µg/mL DNase I (LS002139, Worthington Biochemical)) to digest tumor tissue. The mixture was digested at 37°C for 30 min with a rotation speed of 30 rpm. Then, the tissue digestion was terminated and filtered. The samples were centrifuged, and the supernatants were discarded. The precipitate was resuspended in erythrocyte lysate and placed on ice for 5 min. Precooled PBS was added to the centrifuge tube and washed before proceeding to the staining step.

For staining: a Zombie NIR Fixable Viability Kit (#423105, Biolegend) was used to determine whether the cells were alive or dead. Next, the cells were sealed with serum or TruStain FcX PLUS (anti-mouse CD16/32) antibody (#156603, Biolegend) at 4°C for 10 min and then directly added to the antibody mixture for staining under dark conditions for 30 min. For the staining of T cells, the antibody mixture consisted of a cell staining buffer (#420201, Biolegend) containing working concentrations of Percp/cy5.5-conjugated CD45 (#103132, Biolegend), PB-conjugated CD3ε (#155612, Biolegend), FITC-conjugated CD4 (#100406, Biolegend), and PE-conjugated CD8b (#140408, Biolegend). For the staining of dendritic cells (DCs), the antibody mixture comprised cell staining buffer containing working concentrations of Percp/cy5.5-conjugated CD45 (#103132, Biolegend), FITC-conjugated CD11b (#101206, Biolegend), BV605-conjugated CD11c (#117334, Biolegend), APC-conjugated CD80 (#104714, Biolegend), and BV421-conjugated CD86 (#105123, Biolegend). Cells were washed and resuspended in 300 µL of staining buffer after being stained. Stained cells were analyzed using flow cytometry (Sony SA3800), and the results were processed using FlowJo software.

Immunohistochemistry and multiplex immunohistochemistry

Immunohistochemistry (IHC): Fixed and paraffin-embedded mouse tumor specimens were continuously sectioned, dewaxed, and inactivated with 3% H_2O_2. After the slides were cleaned with PBS, the slides were placed in the citric acid buffer for antigen repair. The tissue samples on the slides underwent immunohistochemical staining, and serum was added to the tissue samples. After sealing at RT for 1 hour, the primary antibody against CD8 (#98941, CST) was added, and samples were incubated at 4°C overnight. After the HRP-conjugated goat anti-rabbit (PV-6001, ZSGB) was incubated at RT for 1 hour. The 3,3-diaminobenzidine tetrahydrochloride plus (DAB+, ZLI-9018, ZSGB) and hematoxylin (ZLI-9610, ZSGB) were used to stain the tissues and nuclei, respectively. The distribution of CD8-positive cells in various tissue slides was observed using an Olympus vs120 virtual slide scanning system.

Multiplex IHC was performed using the Opal 6 color Detection Kit (NEL821001KT, Akoya Biosciences), as previously described.[18] Formaldehyde-fixed and paraffin-embedded sections were heated in an oven at 65°C for 1.5 hours and then deparaffinized and rehydrated with xylene and ethanol. The slides were washed with ddH_2O (1×3 min) and fixed in 10% formalin for 10 min to increase the adhesion of the tissue patch. The slides were then microwave heated in boiling AR6 (pH=6.0) antigen repair solution for 15 min for antigen retrieval. The slides were washed with ddH_2O (1×30 s) and incubated with 3% H_2O_2 for 10 min to block endogenous peroxidases, followed by washing with TBST (3×3 min). Next, the slides were blocked at RT for 10 min with Opal antibody diluent/blocking solution and incubated with primary antibody against CD3 (#78588), CD4 (#25229), CD8 (#98941), cleaved-CASP3 (#9664; all from CST) at RT for 1 hour or at 4°C overnight. The slides were washed in TBST (3×3 min), incubated with goat anti-rabbit IgG (HRP) secondary antibody (ab205718, Abcam) for 10 min, washed in TBST (3×3 min), and treated with fluorophore-4 tyramine signal amplification (TSA) dye (containing Opal 540, Opal 520, Opal 570, and Opal 620 fluorophores) for 10 min. After the first primary antigen staining, microwave treatment with the AR6 antigen repair solution was performed for 15 min to completely remove the antibody complex. Next, the antigens were sequentially labeled with the primary antibody, followed by secondary antibody incubation and TSA visualization, after which all antigens were successfully labeled with different fluorophores. Slides were stained with DAPI for 5 min at RT, washed once with TBST, and sealed with an anti-fluorescence quencher.

The stained slides were scanned using the PerkinElmer Vectra 3 Imaging System, and bright-field and fluorescent images of the entire tissue were obtained. The acquired images were opened using Inform V.2.4 (PerkinElmer) software and subjected to multispectral image analysis, following previously reported methods.[18]

Statistics

Each experiment was independently repeated at least three times. The data are expressed as mean±SEM. Statistical analyses were performed by using the GraphPad Prism V.8 Software (GraphPad Software, San Diego, California, USA). Intergroup differences were assessed using the Student's t-test or analysis of variance. A $p<0.05$ was considered statistically significant (*$p<0.05$; **$p<0.01$).

RESULTS

IR700DX-6T-PDT inhibits CRC progression in vitro and in vivo

To determine the potential phototherapeutic effects of IR700DX-6T-PDT on CRC cells in vitro, CT26 and HCT116 cells were incubated with varying concentrations of the photosensitizer for 16 hours and subjected to varying light intensities, followed by CCK8 analysis. Remarkably, IR700DX-6T-PDT effectively inhibited cancer cell viability in a photosensitizer concentration-dependent and light-dose-dependent manner (figure 1A,B). PI staining was used to assess cell death after IR700DX-6T-PDT. Cells with intact plasma membranes remained unstained. CT26 and HCT116 cells exhibited considerably stronger PI staining than the other control groups on incubation with IR700DX-6T followed by light irradiation, indicating that IR700DX-6T-PDT induced membrane rupture (figure 1C,E). Flow cytometry also showed that PDT-treated cells proceeded to annexin V and PI double-positive stages (figure 1D,F).

We investigated the efficacy of PDT in a CT26 tumor-bearing BALB/c mouse model. IR700DX-6T was introduced into the tumors via tail vein injection and irradiated with light. Tumor progression was monitored by measuring

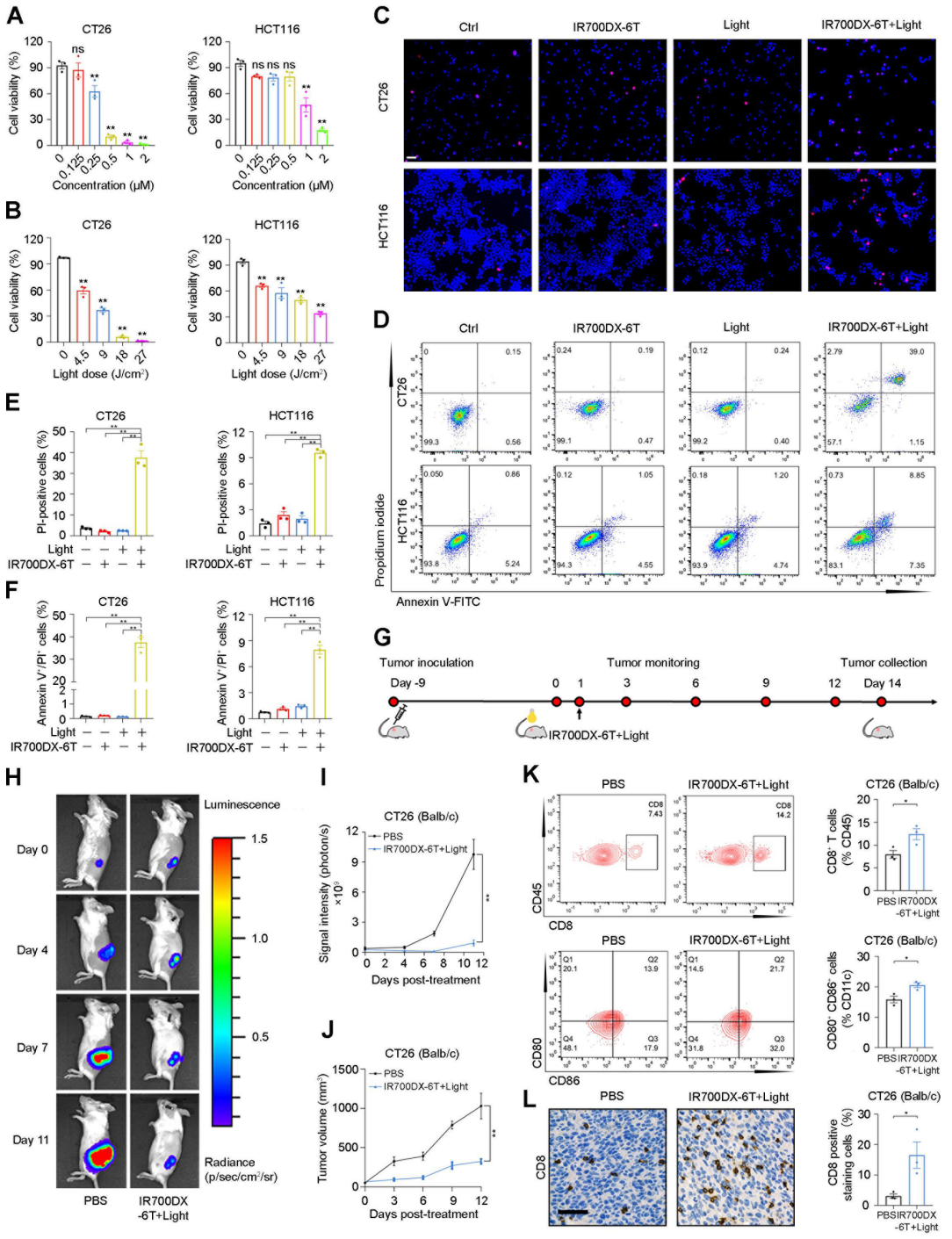

Figure 1 IR700DX-6T-PDT inhibits CRC tumor progression in vitro and in vivo. (A) CT26 and HCT116 cells were incubated with different concentrations of IR700DX-6T (0.125, 0.25, 0.5, 1.0, 2.0 μM) or controls for 16 hours, followed by light irradiation at 27 J/cm^2 before CCK8 analysis. (B) Cells were treated with 1.0 μM photosensitizer for 16 hours, and subjected to various light doses (4.5, 9.0, 18, 27 J/cm^2) before cell viability was tested. (C–F) After cells were subjected to IR700DX-6T (1.0 μM) and light irradiation (18 J/cm^2 with CT26 and 27 J/cm^2 with HCT116), Hoechst33342/PI double staining (C, E) and Annexin V-FITC/PI dual-staining assay (D, F) were used to evaluate cell death. Scale bar, 50 μm. (G) Schematic illustration of IR700DX-6T-PDT in vivo. CT26-fLuc cells were subcutaneously injected into the flanks of each mouse. Tumor-bearing mice were randomized into two groups, including PBS and IR700DX-6T+Light groups. Light irradiation at a dosage of 18 J/cm^2 was applied to the IR700DX-6T+Light group. Representative BLI of BALB/c mice during PDT treatment (H) and quantified BLI from tumors (n=5) (I). (J) Tumor growth curves of the treatment and control groups (n=5). (K) Representative flow cytometric analysis and quantitative analyses of CD8 toxic T cell infiltration (above, the proportion of CD8$^+$ cells in the CD45$^+$ populations) and the maturation level of DCs (below, the proportion of CD86 and CD80 double-positive cells in the CD11c$^+$ populations) in the single-cell suspension of murine tumors at the end of treatment (n=3). (L) IHC analysis of CD8 expression in tumors (n=3). Scale bar, 50 μm. Data are expressed as mean±SEM. ns, not significant, *p<0.05; **p<0.01. BLI, bioluminescence images; CRC, colorectal cancer; DC, dendritic cell; PDT, photodynamic therapy; PI, propidium iodide; PBS, phosphate buffered saline.

tumor volume and BLI every 3 days (figure 1G). Compared with the control group, tumor growth was significantly delayed in the IR700DX-6T with light irradiation group, and at the end of the treatment, the tumors were considerably smaller (figure 1H–J). Moreover, IR700DX-6T-PDT had no effect on murine body weight, indicating minimal side effects (online supplemental figure 1A).

DCs are specialized antigen-presenting cells that play a crucial role in antitumor immunity by presenting antigens to $CD8^+$ T cells and inducing tumor cell death.[16 19] We found that at 14 days, the percentage of mature DCs ($CD80^+CD86^+$) was significantly elevated in the tumors of IR700DX-6T-PDT-treated mice, suggesting that PDT stimulated DC accumulation and maturation. In addition, the PDT group exhibited a 1.6-fold increase in $CD8^+$ tumor-infiltrating T lymphocytes compared with the control group (figure 1K). IHC analysis showed that the density of $CD8^+$ T cell infiltration in the tumors treated with PDT was significantly higher than that in the control group, indicating the ability of IR700DX-6T-PDT to promote $CD8^+$ T cell infiltration into tumors (figure 1L).

Furthermore, to determine the effect of IR700DX-6T-PDT on tumor reduction is dependent on host immune responses, CT26 cells were subcutaneously inoculated into immunocompetent BALB/c mice and T-cell deficient BALB/c-nu/nu (nude) mice, and treated with IR700DX-6T-PDT or PBS. Although IR700DX-6T-PDT treatment reduced tumor growth and tumor weight in both BALB/c mice and nude mice (online supplemental figure 1B, C), higher tumor reduction rates of tumor growth and tumor weight were observed in IR700DX-6T-PDT-treated BALB/c mice than in IR700DX-6T-PDT-treated nude mice (online supplemental figure 1D), indicating that IR700DX-6T-PDT induced anticancer immune responses and that its efficacy depends on host immunity. In addition, IR700DX-6T-PDT treatment had no effect on murine body weight of each group (online supplemental figure 1E).

IR700DX-6T-PDT induces CRC cell pyroptosis via GSDME cleaved by activated CASP3

To determine the type of cell death induced by IR700DX-6T-PDT, we examined the morphological changes in the cells following treatment. After irradiation, the cells showed pericellular swelling and bubble-like protrusions on the membrane, which are classic hallmarks of pyroptotic cells (figure 2A). The release of intracellular LDH could serve as an indicator for evaluating pyroptosis-related cytotoxicity.[20] Indeed, a substantial amount of LDH was detected in the supernatant of cells treated with IR700DX-6T on irradiation, while the control cells exhibited minimal LDH release (figure 2B). The gasdermins (GSDMs) family is a pore-forming effector protein that causes cell membrane permeabilization and pyroptosis. Next, we investigated the gasdermin responsible for IR700DX-6T-PDT-induced pyroptosis. Western blot analysis showed the release of the N-terminal fragment of GSDME (GSDME-N) in CT26 and HCT116 cells following IR700DX-6T-PDT, whereas no GSDMD cleavage was observed, indicating that IR700DX-6T-PDT induced GSDME-dependent pyroptosis in CRC cells (figure 2C). To further elucidate the pivotal role of GSDME in IR700DX-6T-PDT-induced pyroptosis, we silenced GSDME expression in CT26 and HCT116 cells using siRNA (figure 2D). In contrast to IR700DX-6T-PDT-treated NC cells, GSDME knockdown resulted in decreased expression of GSDME-N protein and reduced LDH levels (figure 2E,F). These findings indicate that IR700DX-6T-PDT-induced pyroptosis is mediated by the key pyroptosis-executing protein, GSDME.

Studies have shown that the CASP3/GSDME signaling pathway mediates the interconversion between tumor cell apoptosis and pyroptosis.[21] Interestingly, treatment with IR700DX-6T-PDT significantly increased cleaved-CASP3 expression (figure 3A). Pretreatment with Ac-DEVD-CHO, a specific inhibitor of CASP3, prevented the activation of CASP3, inhibited the cleavage of GSDME, and attenuated the release of LDH in CT26 and HCT116 cells on IR700DX-6T-PDT (figure 3B,C). When CASP3 was inhibited by Ac-DEVD-CHO, swollen pyroptotic cells were barely observed in the IR700DX-6T-PDT group, as shown in figure 3D,E. Collectively, these data indicated that pyroptosis induced by IR700DX-6T-PDT is mediated through active CASP3 cleavage of GSDME.

ROS/p38 pathway-mediated GSDME-dependent pyroptosis induced by IR700DX-6T-PDT

ROS generated by PDT are the active forms of oxygen that can impede cellular growth and damage cells. DCFH-DA and MitoSox red fluorescent probes were used to detect the total and mitochondrial ROS generated by IR700DX-6T-PDT. We found that both the total and mitochondrial ROS levels were dramatically increased in CRC cells after IR700DX-6T-PDT. Pretreatment with N-acetyl-L-cysteine (NAC), a potent ROS scavenger, effectively attenuated the elevated ROS levels and markedly abolished cleaved-CASP3 and GSDME-N expression in CT26 and HCT116 cells, indicating that ROS was the primary cause of IR700DX-6T-PDT-induced pyroptosis (figure 4A–C and online supplemental figure 2A).

ROS are known to modulate the signaling pathways of mitogen-activated protein kinase (MAPK),[22 23] we, therefore, studied the effect of IR700DX-6T-PDT on MAPK pathway. Both JNK and p38, especially p38, were phosphorylated on IR700DX-6T-PDT in CT26 and HCT116 cells, compared with the control groups. However, the expression of p-MEK and p-ERK increased exclusively in CT26 cells but remained unchanged in HCT116 cells (figure 4D). Next, we found that NAC pretreatment resulted in significantly reduced p38 phosphorylation but did not show a notable impact on the other MAPKs (figure 4E and online supplemental figure 2B).

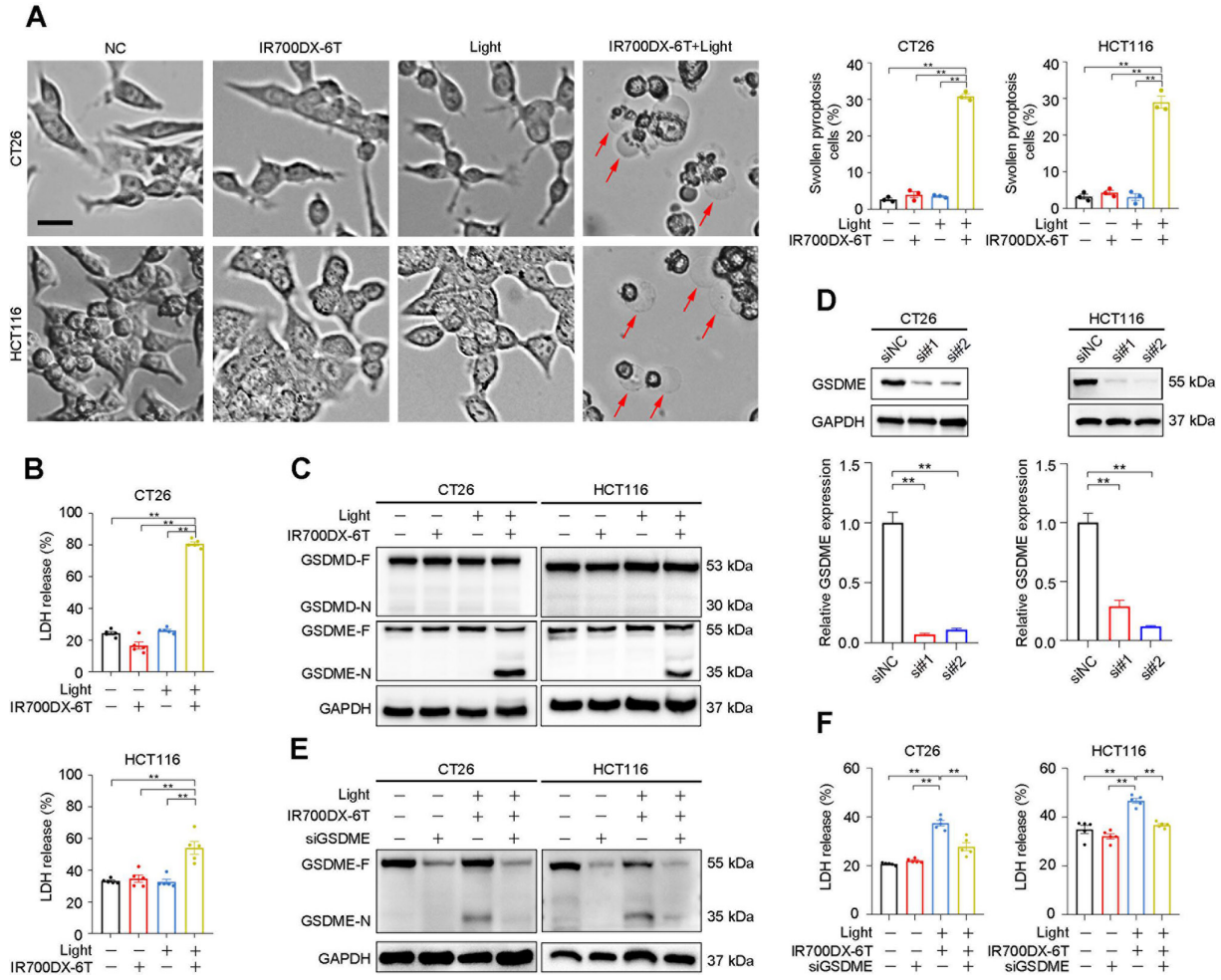

Figure 2 GSDME but not GSDMD is cleaved in IR700DX-6T-PDT induced pyroptosis in CRC. (A) Representative bright-field microscopy images (left) and corresponding quantitative analyses (right) of CT26 and HCT116 cells treated with IR700DX-6T-PDT. The red arrows represent pyroptotic cells. Scale bars, 20 µm. (B) Cytotoxicity was detected using the release of LDH in the culture supernatants. (C) Western blot analysis of GSDMD and GSDME expression in CT26 and HCT116 cells. (D) qPCR (below) and Western blot analysis (above) shows the silencing efficiency of siRNA against GSDME. (E) GSDME expression was examined after CT26 and HCT116 cells were transfected with GSDME or control siRNA, and subjected to IR700DX-6T-PDT. (F) LDH release was evaluated using the LDH release kit. Data are expressed as mean±SEM.**p<0.01. CRC, colorectal cancer; GSDMD-F, gasdermin E-full length; GSDMD-N, GSDMD N-terminal fragment; LDH, lactate dehydrogenase.

To clarify the regulatory effect of p38 pathways on IR700DX-6T-PDT-induced pyroptosis in CRC, cells were preincubated with a p38 inhibitor (SB202190), which effectively reversed the activation of GSDME-N and cleaved-CASP3, as well as the release of LDH caused by IR700DX-6T-PDT (figure 4F,G and online supplemental figure 2C). Morphologically, incubation with SB202190 inhibited the formation of IR700DX-6T-PDT-induced cell bubbles, indicating that the p38 inhibitor could effectively reduce the pyroptosis induced by PDT (figure 4H). These results indicated that p38 signaling acted as a major upstream regulator of CASP3/GSDME-dependent pyroptosis induced by IR700DX-6T-PDT.

Efficacy of IR700DX-6T-PDT in sensitizing MSS-type CRC tumors to anti-PD-1 treatment

Recent clinical data indicate that immunotherapy, especially ICIs, is ineffective against most CRC tumors. Approximately 85% of patients with CRC have pMMR or MSS tumors that do not respond to ICIs.[3 24] Therefore, we investigated whether IR700DX-6T-PDT could enhance the efficacy of PD-1 blockade in a syngeneic mouse model with CT26 cells expressing firefly luciferase (CT26-fLuc; figure 5A). With negligible side effects of this treatment, as demonstrated by the body weights in figure 5B, the IR700DX-6T-PDT+PD-1 blockade exhibited a strong tumor inhibition capacity. Tumor growth was significantly inhibited in IR700DX-6T-PDT combined with anti-PD-1 compared with the individual administration of anti-PD-1 or PDT (figure 5C). Both tumor volume and weight were significantly reduced in the combination treatment group compared with the control groups (figure 5D,E). DCs are essential antigen-presenting cells that serve as the first line of defense against tumors and play a pivotal role in antitumor immunity. We found that the amount of matured DCs

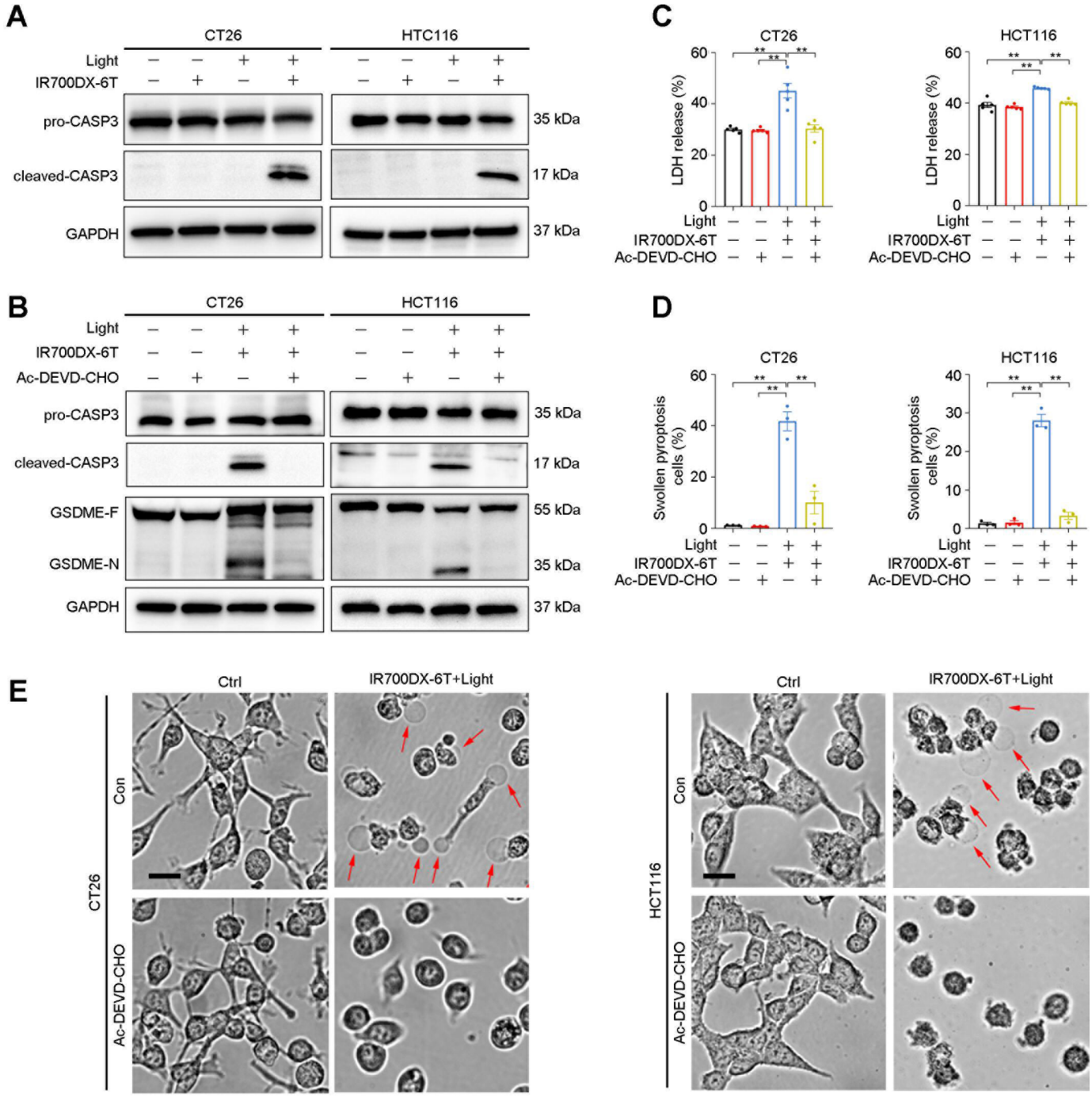

Figure 3 GSDME cleaved by activated CASP3 mediates IR700DX-6T-PDT to causes pyroptosis of tumor cells. (A) Western blot analysis of CASP3 expression in CT26 and HCT116 cells subjected to IR700DX-6T-PDT. (B) CASP3 and GSDME expression in each group of CT26 and HCT116 cells treated with IR700DX-6T-PDT in the presence or absence of Ac-DEVD-CHO. (C) Effect of CASP3 inhibitor on LDH release on IR700DX-6T-PDT treatment. (D, E) The morphological features of pyroptosis were detected in different treatment groups of CT26 and HCT116 cells through light microscopy. Red arrows represent pyroptotic cells. Scale bar, 20 µm. Data are presented as mean±SEM. **p<0.01. CASP3, caspase3; GSDME-F, gasdermin E-full length; GSDME-N, GSDME N-terminal fragment; LDH, lactate dehydrogenase; PDT, photodynamic therapy.

($CD80^+CD86^+/CD11c^+$) and cytotoxic T cells ($CD8^+/CD45^+$) increased dramatically in the combinational treatment group compared with the individual treatment groups, indicating that the combination therapy could recruit more matured DCs and killer T cells to the tumor site, thus improving the immune microenvironment of MSS-type "cold" tumors (figure 5F,G). Multiplex IHC analysis of the tumors also indicated increased infiltration of CD3-positive, CD4-positive, CD8-positive T cells and cleaved-CASP3 expression in response to IR700DX-6T-PDT and anti-PD-1 on the 15th day (figure 5H,I). These data suggest that IR700DX-6T-PDT stimulated the antitumor immune response through DC maturation and cytotoxic T cell

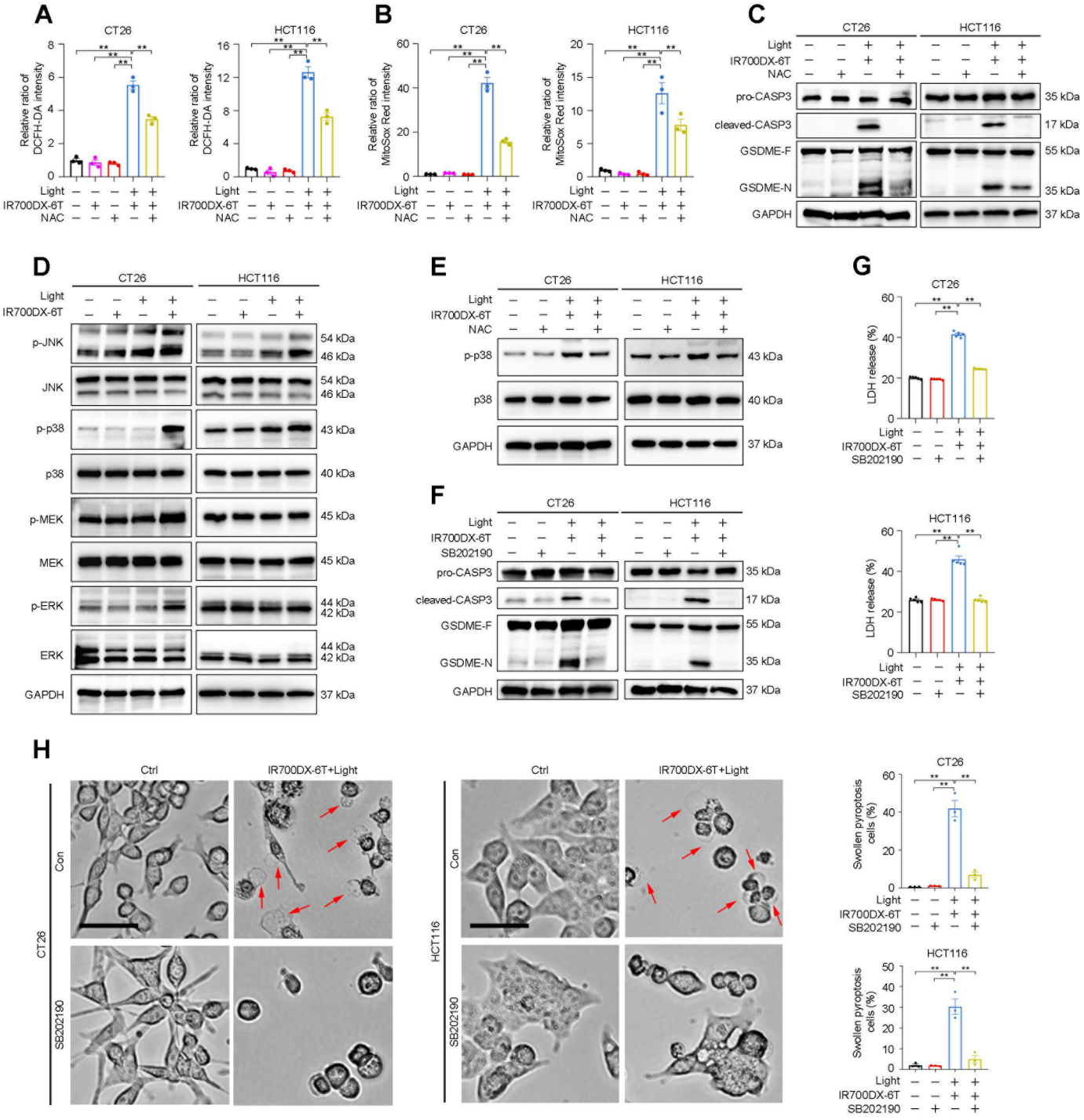

Figure 4 ROS/MAPK pathway mediates GSDME dependent pyroptosis induced by IR700DX-6T-PDT. (A) ROS levels in CT26 and HCT116 cells were detected using a DCFH-DA fluorescence probe. (B) Mitochondrial ROS expression level was detected by flow cytometry using MitoSox Red staining. (C) Western blot analysis of pyroptosis-related protein expression (GSDME-F, GSDME-N, pro-CASP3, and cleaved-CASP3) in CT26 and HCT116 cells after NAC pretreatments. (D) Phosphorylation of JNK, p38, MEK, and ERK in different treatment groups. (E) p38 phosphorylation in CT26 and HCT116 cells treated with IR700DX-6T-PDT in the presence or absence of NAC. (F) GSDME and CASP3 expression in cells were pretreated with p38 inhibitor SB202190 and subject to PDT. (G) LDH release level of CT26 and HCT116 cells treated with or without IR700DX-6T-PDT and p38 inhibitor. (H) The indicated cells were preincubated with p38 inhibitor for 4 hours and subjected to IR700DX-6T-PDT. Cell pyroptosis and morphological changes were observed. Red arrows represent pyroptotic cells. Scale bar, 50 µm. Data are expressed as mean±SEM. *p<0.05; **p<0.01. CASP3: caspase-3; GSDME-F, gasdermin E-full length; GSDME-N, GSDME N-terminal fragment; LDH, lactate dehydrogenase; NAC, N-acetyl-L-cysteine; ROS, reactive oxygen species.

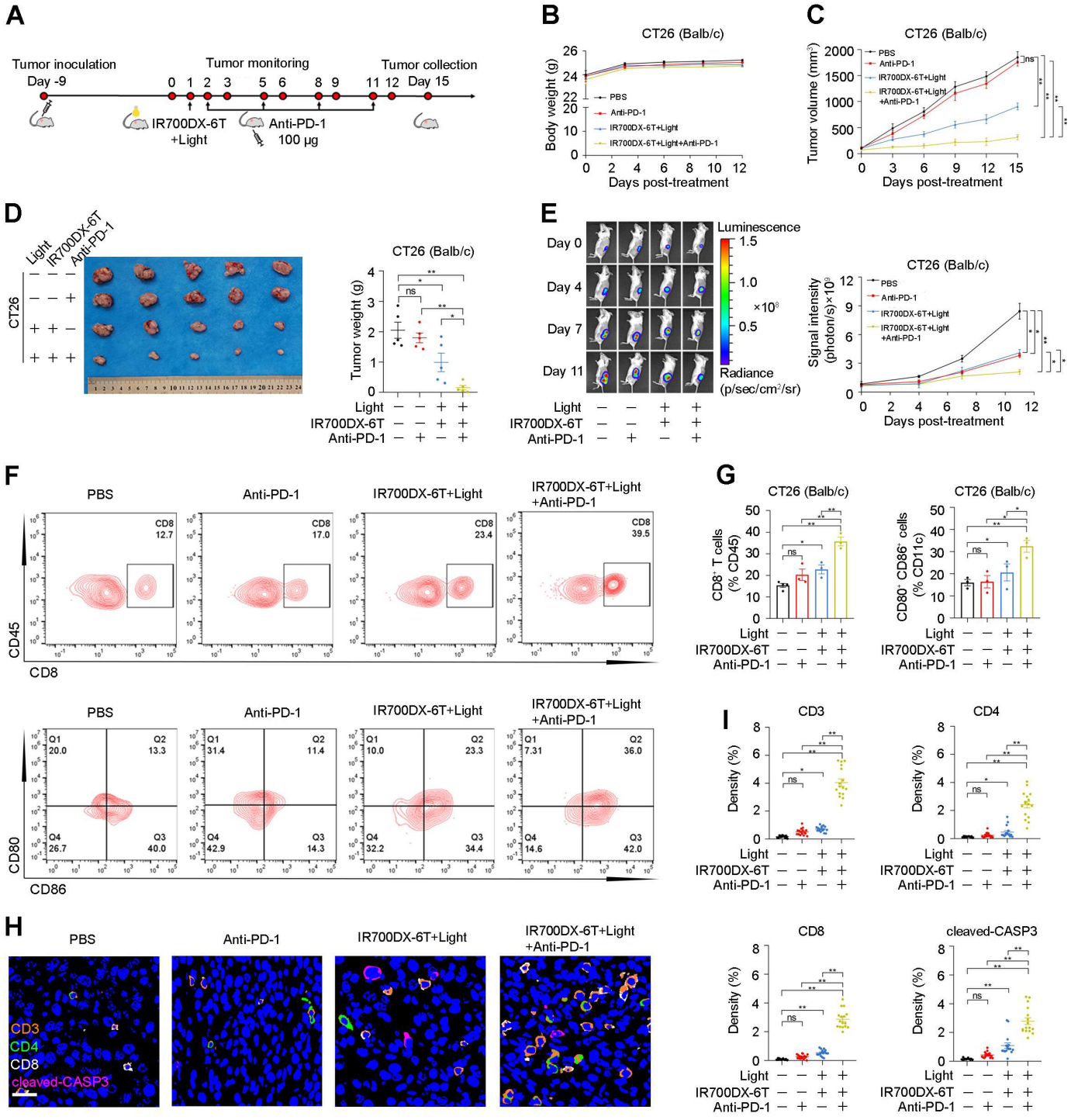

Figure 5 IR700DX-6T-PDT sensitizes PD-1 blockade in MSS-CRC tumors. (A) Schematic illustration of combinational treatment of IR700DX-6T-PDT and PD-1 blockade. Ten days after the subcutaneous injection of CT26-fLuc cells into mice, PDT treatment was applied. One day later, 100 μg of anti-PD-1 antibody was injected into the abdominal cavity of mice, and then PD-1 blockade treatment was conducted every 3 days, a total of four times. Body weight (B), tumor growth curves (C), and tumor weight (D) were examined in different treatment groups (n=5 mice/group). (E) Representative BLI of indicated groups of BALB/c mice during PDT treatment (left) and radiance measurements (right; n=5). (F, G) Ratios of $CD8^+$ cells (above) and $CD80^+CD86^+$ cells (below) were detected at the end of treatment (n=3). (H) Representative images of multiplex IHC staining. Quantification is shown in (I) (n=16). CD3: orange; CD4: green; CD8: white; cleaved-CASP3: pink; DAPI: blue. Scale bar, 20 μm. Data are presented as mean±SEM *p<0.05; **p<0.01. CRC, colorectal cancer; BLI, bioluminescence images; cleaved-CASP3, cleaved-caspase3; MSS, microsatellite stable; PDT, photodynamic therapy; PBS, phosphate buffered saline.

proliferation, thereby sensitizing MSS type CRC to anti-PD-1 treatment

GSDME demethylation enhances IR700DX-6T-PDT-induced pyroptosis and facilitates its antitumor effect

Dysregulation of epigenetic modifications, especially DNA methylation, is a hallmark of cancer.[25] GSDME is aberrantly methylated in CRC, resulting in decreased expression compared with that in normal cells.[26] Decitabine is a commonly used DNA methyltransferase inhibitor that allows for DNA hypomethylation.[27] Therefore, we tested whether decitabine, as a preconditioning agent, could sensitize cancer cells with GSDME methylation to IR700DX-6T-PDT. Among several CRC cell lines, SW620 and HCT15 cells were selected because of their low endogenous expression of GSDME (online supplemental figure 3A). Following decitabine treatment, we observed elevated levels of GSDME mRNA and protein expression on the second and sixth day in SW620 and HCT15 cells, respectively (figure 6A and online supplemental figure 3B, C). Decitabine pretreated cells were more responsive to IR700DX-6T-PDT, as evidenced by the release of LDH (figure 6B and online supplemental figure 3D), indicating that GSDME demethylation promoted IR700DX-6T-PDT-induced pyroptosis.

Low GSDME expression was observed in 4T1 mouse breast cancer cells.[27] Similar to SW620 and HCT15 cells, 4T1 cells showed elevated levels of GSDME after being pretreated with decitabine (figure 6C,D). We next studied the effect of combined IR700DX-6T-PDT and decitabine pretreatment on enhancing the efficacy of PD-1 blockade in 4T1 subcutaneous tumor-bearing BALB/c mice (figure 6E). Although tumor growth was comparable between PDT alone or in combination with decitabine treatment, suggesting an immunosuppressive microenvironment within the 4T1 tumors, the combination of decitabine, IR700DX-6T-PDT, and anti-PD-1 antibody resulted in the most significant tumor regression (figure 6G,F). The most notable increase in $CD8^+$ T cells and $CD80^+CD86^+$ DCs was detected in the triplet therapy group compared with the other treatment or control groups (figure 6H). Multiplex IHC analysis of the tumor on the 15th day identified dramatically increased cytotoxic T lymphocyte (CTL) infiltration and cleaved-CASP3 in response to decitabine, IR700DX-6T-PDT and PD-1 blockade (figure 6I). No evidence of normal tissue toxicity was detected in the liver or kidneys as evidenced by H&E staining (online supplemental figure 3E). These results demonstrated that decitabine enhanced the efficiency of IR700DX-6T-PDT-induced pyroptosis by demethylating GSDME, thereby boosting the antitumor immune response of IR700DX-6T-PDT in combination with PD-1 blockade.

DISCUSSION

In this study, we elucidated the phototherapeutic effects of TSPO-targeted PDT on pyroptosis in CRC. Pyroptosis, a newly disclosed form of programmed cell death, is fundamentally proinflammatory and plays a critical role in immune responses.[11 28] A mitochondrial outer membrane protein called TSPO is an evolutionarily conserved transmembrane protein that is implicated in the regulation of oxidative stress, iron homeostasis, cholesterol transport, and inflammatory response.[8] The high expression of TSPO in various cancers renders it a promising target specific to tumors, given its involvement in tumor progression and unfavorable prognosis.[29] In our previous study, we developed a TSPO-targeted photosensitizer, IR700DX-6T, which resulted in breast cancer cell death accompanied by significant mitochondrial damage on PDT, leading to efficient and target-specific tumor regression.[10] However, the precise role of IR700DX-6T-PDT in modulating tumor cell death remained largely unknown. Here, we showed that IR700DX-6T-PDT induces GSDME-dependent pyroptosis in CRC. PDT reportedly triggered cell death depending on the subcellular localization of the photosensitizer and the degree of photodamage.[30 31] Mitochondria-anchored photosensitizer-mediated PDT triggered pyroptosis in cervical and breast cancer cells, revealing that mitochondria-targeted PDT seemingly prompted a higher degree of pyroptosis.[32 33] Another study also reported that TSPO deficiency exacerbated GSDMD-induced macrophage pyroptosis in inflammatory bowel disease,[34] which is consistent with our results.

Our findings raise questions regarding the mechanism underlying IR700DX-6T-PDT-mediated pyroptosis in CRC cells through GSDME cleavage. Previous studies have reported that the efficacy of PDT depends on ROS generation, which plays a pivotal role in pyroptosis.[35 36] Our results revealed that ROS accumulated in CRC cells on IR700DX-6T-PDT treatment, and the expression of cleaved-CASP3 and GSDME-N was inhibited by NAC, indicating that the pyroptosis signal was initiated by ROS on IR700DX-6T-PDT treatment. The MAPK pathway is activated by oxidative stress, endoplasmic reticulum stress, cytokines, and other stimuli. It plays an important role in CRC progression.[37 38] In this study, we found that the p38 pathway was activated on PDT and that NAC treatment effectively suppressed the phosphorylation level of p38 and the degree of pyroptosis, indicating that ROS served as upstream regulators of p38. Therefore, we concluded that IR700DX-6T-PDT triggers pyroptosis in CRC by activating the ROS/p38/CASP3/GSDME signaling pathway.

Cancer immunotherapy has rapidly evolved into a mature treatment strategy for tumors. Checkpoint blockade, such as PD-L1/PD-1 or CTLA-4 blockade, conferred major clinical benefit to patients with CRC with MMR-deficient and microsatellite instability-high.[39] Nonetheless, singlet PD-1 blockade is inefficient in most patients with CRC with pMMR/MSS because of limited neoantigen repertoire and an immune-excluded or immune-desert tumor microenvironment with deficient or inactive tumor-infiltrating lymphocytes.[40 41] Here, we found that IR700DX-6T-PDT sensitizes the immune response of MSS-CRC to PD-1 blockade by inducing

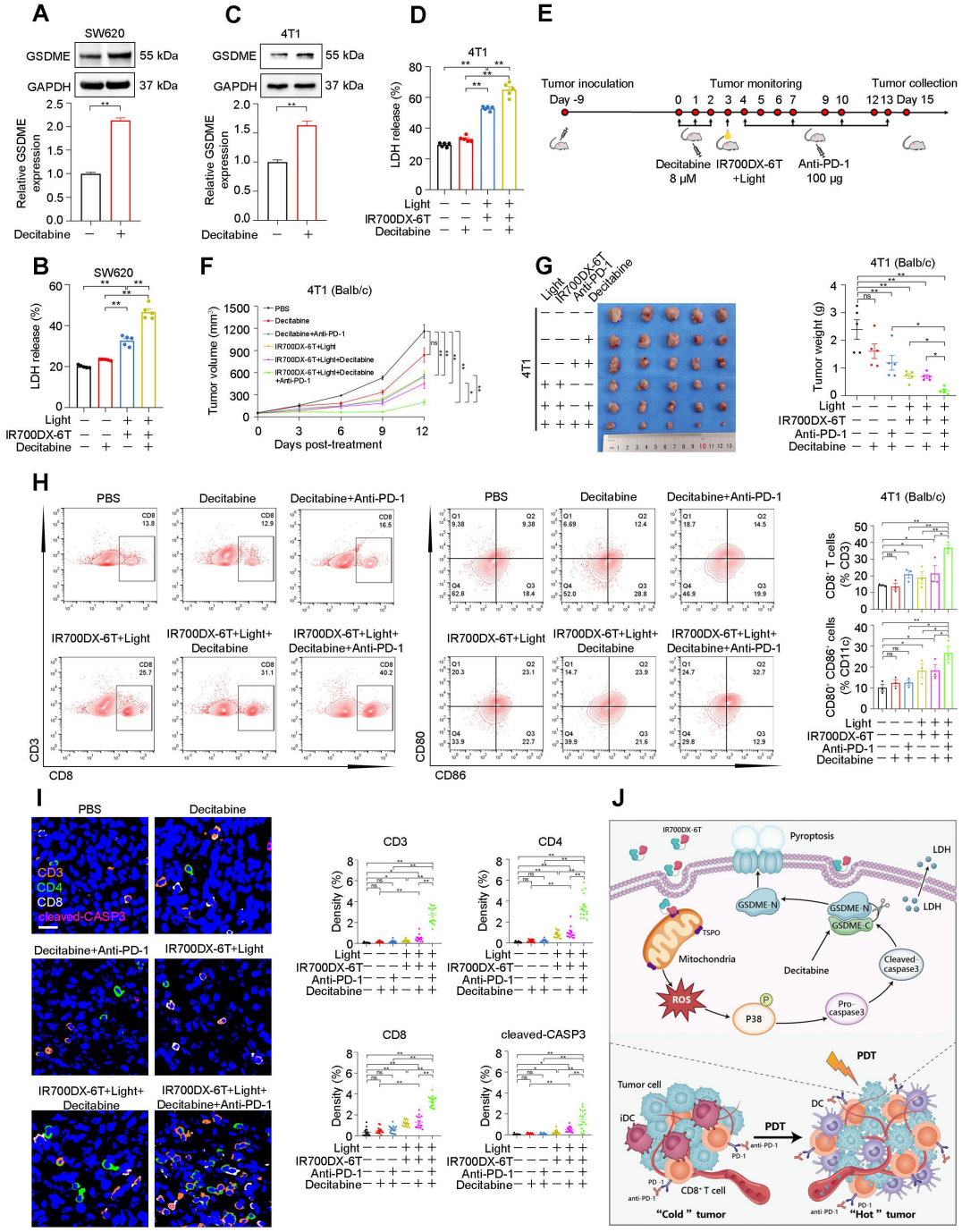

Figure 6 Demethylation of GSDME expression enhances IR700DX-6T-PDT sensitivity and improves the antitumor efficacy of IR700DX-6T-PDT in combination with PD-1 blockade. (A) SW620 cells was treated with 5 μM decitabine for 2 days and then GSDME mRNA (below) and protein (above) levels were assessed by qPCR and Western blot, respectively. (B) SW620 cells with low endogenous GSDME expression were treated with 5 μM decitabine and IR700DX-6T-PDT, and then analyzed for LDH release. (C) Expressions of GSDME mRNA (below) and protein (above) levels in 4T1 cells after having been treated with 1.25 μM decitabine for 5 days. (D) LDH release of 4T1 cells after indicated treatment. (E) Schematic illustration of the experimental timeline for tumor inoculation and combination treatment with decitabine, IR700DX-6T, and anti-PD-1 antibody. The 4T1 tumor-bearing mice were treated with PBS, decitabine, decitabine+anti-PD-1, IR700DX-6T+light, IR700DX-6T+light+decitabine, IR700DX-6T+light+decitabine+anti-PD-1, respectively (doses: decitabine, 80 μM, 3 times; anti-PD-1, 100 μg, 4 times; IR700DX-6T+light, 7.5 nM IR700DX-6T, light irradiation 18 J/cm^2). (F) Growth curves of tumors after various treatments (n=5). (G) Tumor weight in a subcutaneous 4T1 murine model (n=5). (H) Representative flow cytometry analysis (left) and proportions (right) of CD8$^+$ T cells and CD80$^+$CD86$^+$ cells within the tumor (n=3). (I) Multiplex IHC (CD3, CD4, CD8, and cleaved-CASP3) of tumor tissues after different treatments (n=16). CD3: orange; CD4: green; CD8: white; cleaved-CASP3: pink; DAPI: blue. Scale bar, 20 μm. (J) The proposed working model. IR700DX-6T-mediated PDT induces pyroptosis and boosts antitumor immunity. Data are presented as mean±SEM. **p<0.01. cleaved-CASP3, cleaved-caspase3; GSDME, gasdermin E; IHC, immunohistochemistry; LDH, lactate dehydrogenase; PDT, photodynamic therapy; PBS, phosphate buffered saline.

pyroptosis. Tumor cells undergoing pyroptosis may secrete IL-1β, IL-18, and HMGB1, trigger ICD, and activate immune cells such as DCs, macrophages, natural killer cells, etc. This process induces CTL infiltration, thereby promoting antitumor effects by converting "cold" tumors into "hot" tumors.[42–44] Our results indicated that IR700DX-6T-PDT stimulated DC maturation and CTL recruitment, improved the immune microenvironment of CT26 transplanted "cold" tumor, and enhanced the efficacy of PD-1 blockade. Notably, pyroptosis may exhibit both antitumor and tumor-promoting effects, hindering the clinical application of agents targeting pyroptosis, such as metformin, paclitaxel, and anthocyanin.[45] IR700DX-6T-PDT, as a novel tumor-targeted pyroptosis inducer, could avoid the pyroptosis of immune cells and damage to adjacent or normal tissues, rendering it a promising future cancer therapeutic strategy either to be applied alone or in combination with immunotherapy.

Methyltransferase inhibitors and other epigenetic drugs can restore the expression of several genes. Decitabine, a classic methyltransferase inhibitor, significantly increased GSDME expression and induced pyroptosis in SW620 and HCT15 cells on IR700DX-6T-PDT treatment. Decitabine, either used alone or in combination, could significantly inhibit the progression of non-small cell lung cancer and gastric cancer.[46 47] In addition, decitabine plays an important role in immune regulation, such as enhancing the expression of costimulatory molecules, major histocompatibility complex class I and other immune markers on tumor cells, improving the antitumor response of $CD8^+$ T cells, and reducing the depletion of CAR T cells after antigen exposure.[48–50] In this study, we explored the antitumor effect of decitabine treatment in CRC by amplifying IR700DX-6T-PDT-induced pyroptosis. Expectedly, IR700DX-6T-PDT partially inhibited tumor progression in 4T1 cells with low endogenous GSDME expression, whereas in combination with decitabine and an anti-PD-1 antibody, the triplet treatment induced dramatic tumor shrinkage and immune cell infiltration. As a clinically applicable drug, decitabine shows great potential for promoting pyroptosis in tumors with low endogenous GSDME expression on IR700DX-6T-PDT treatment.

CONCLUSIONS

In summary, our study demonstrated that IR700DX-6T-PDT induced pyroptosis in CRC via the ROS/p38/CASP3/GSDME axis and that IR700DX-6T-PDT could sensitize MSS-CRC to PD-1 blockade treatment. Decitabine served as a pretreatment adjuvant in combination with IR700DX-6T-PDT and PD-1 blockade to enhance the antitumor response in tumors with low endogenous GSDME expression (figure 6J). Therefore, IR700DX-6T-PDT may serve as a novel therapeutic strategy to target GSDME in MSS-CRC. The ROS/p38/CASP3/GSDME axis shows promise as a potential therapeutic target for CRC treatment.

Author affiliations
[1]Department of Gastroenterology, Tangdu Hospital, Fourth Military Medical University, Xi'an, Shaanxi, China
[2]State Key Laboratory of Holistic Integrative Management of Gastrointestinal Cancers, Xijing Hospital of Digestive Diseases, Fourth Military Medical University, Xi'an, Shaanxi, China
[3]College of Life Sciences, Northwest University, Xi'an, Shaanxi, China
[4]Department of Gastroenterology, The 980th Hospital of the PLA Joint Logistics Support Force (Primary Bethune International Peace Hospital of PLA), Shijiazhuang, Hebei, China
[5]Department of Pancreatic Hepatobiliary Surgery, The Sixth Affiliated Hospital, Sun Yat-sen University, Guangzhou, Guangdong, China
[6]Department of Biochemistry and Molecular Biology, Fourth Military Medical University, Xi'an, Shaanxi, China
[7]Vanderbilt University Institute of Imaging Sciences, Vanderbilt University Medical Center, Nashville, Tennessee, USA

Acknowledgements We thank Qing Xie from the Vanderbilt University Institute of Imaging Sciences for the technical assistance with PDT.

Contributors YL, XZ and XW conceived and designed the experiment. YZ, WZ, BW, PW, DL, and TC completed the experiment. YZ and WZ conducted the data analysis and interpreted the results. YZ, DZ, HH and MB wrote and edited the paper. YL and XZ supervised and coordinated all aspects of the work. All authors read and approved the final manuscript. YL and XZ are responsible for the overall content as guarantor.

Funding This work was supported by grants from the National Natural Science Foundation of China (NO. 82273142, 82222058, 82173256, 81972224, 82073197); National Key R&D Program of China (NO. 2022YFC2505104); the State Key Laboratory of Holistic Integrative Management of Gastrointestinal cancers (NO. CBSKL2022ZZ55).

Competing interests None declared.

Patient consent for publication Not applicable.

Ethics approval Ethics approval and consent to perform animal studies were approved by the Institutional Animal Care and Use Committee of the Fourth Military Medical University (IACUC20210615). All methods were performed in accordance with relevant guidelines.

Provenance and peer review Not commissioned; externally peer reviewed.

Data availability statement All data relevant to the study are included in the article or uploaded as online supplemental information.

ORCID iD
Yuanyuan Lu http://orcid.org/0000-0003-0194-8074

REFERENCES

1 Li N, Lu B, Luo C, *et al*. Incidence, mortality, survival, risk factor and screening of colorectal cancer: a comparison among China, Europe, and Northern America. *Cancer Lett* 2021;522:255–68.
2 Sung JJY, Chiu H-M, Jung K-W, *et al*. Increasing trend in young-onset colorectal cancer in Asia: more cancers in men and more rectal cancers. *Am J Gastroenterol* 2019;114:322–9.

3 Lizardo DY, Kuang C, Hao S, *et al*. Immunotherapy efficacy on mismatch repair-deficient colorectal cancer: from bench to bedside. *Biochim Biophys Acta Rev Cancer* 2020;1874:188447.
4 Biller LH, Schrag D. Diagnosis and treatment of metastatic colorectal cancer: a review. *JAMA* 2021;325:669.
5 Zhao X, Liu J, Fan J, *et al*. Recent progress in photosensitizers for overcoming the challenges of photodynamic therapy: from molecular design to application. *Chem Soc Rev* 2021;50:4185–219.
6 Correia JH, Rodrigues JA, Pimenta S, *et al*. Photodynamic therapy review: principles, photosensitizers, applications, and future directions. *Pharmaceutics* 2021;13:1332.
7 Yue D, Cai X, Fan M, *et al*. An alternating irradiation strategy-driven combination therapy of PDT and RNAi for highly efficient inhibition of tumor growth and metastasis. *Adv Healthc Mater* 2021;10:e2001850.
8 Betlazar C, Middleton RJ, Banati R, *et al*. The Translocator protein (TSPO) in mitochondrial bioenergetics and immune processes. *Cells* 2020;9:512.
9 Nutma E, Ceyzériat K, Amor S, *et al*. Cellular sources of TSPO expression in healthy and diseased brain. *Eur J Nucl Med Mol Imaging* 2021;49:146–63.
10 Zhang S, Yang L, Ling X, *et al*. Tumor mitochondria-targeted photodynamic therapy with a Translocator protein (TSPO)-specific photosensitizer. *Acta Biomater* 2015;28:160–70.
11 Wei X, Xie F, Zhou X, *et al*. Role of pyroptosis in inflammation and cancer. *Cell Mol Immunol* 2022;19:971–92.
12 Elias EE, Lyons B, Muruve DA. Gasdermins and pyroptosis in the kidney. *Nat Rev Nephrol* 2023;19:337–50.
13 Hou J, Hsu J-M, Hung M-C. Molecular mechanisms and functions of pyroptosis in inflammation and antitumor immunity. *Mol Cell* 2021;81:4579–90.
14 Gao W, Wang X, Zhou Y, *et al*. Autophagy, ferroptosis, pyroptosis, and necroptosis in tumor immunotherapy. *Signal Transduct Target Ther* 2022;7:196.
15 Xia Y, Jin Y, Cui D, *et al*. Antitumor effect of simvastatin in combination with DNA methyltransferase inhibitor on gastric cancer via GSDME-mediated pyroptosis. *Front Pharmacol* 2022;13:860546.
16 Gao L, Zhang C, Gao D, *et al*. Enhanced anti-tumor efficacy through a combination of integrin Αvβ6-targeted photodynamic therapy and immune checkpoint inhibition. *Theranostics* 2016;6:627–37.
17 Yang L, Zhang S, Ling X, *et al*. Multilayer photodynamic therapy for highly effective and safe cancer treatment. *Acta Biomater* 2017;54:271–80.
18 He Y, Han Y, Fan A, *et al*. Multi-perspective comparison of the immune microenvironment of primary colorectal cancer and liver metastases. *J Transl Med* 2022;20:454.
19 Murphy TL, Murphy KM. Dendritic cells in cancer immunology. *Cell Mol Immunol* 2022;19:3–13.
20 Xia W, Li Y, Wu M, *et al*. Gasdermin E deficiency attenuates acute kidney injury by inhibiting pyroptosis and inflammation. *Cell Death Dis* 2021;12:139.
21 Jiang M, Qi L, Li L, *et al*. The caspase-3/GSDME signal pathway as a switch between apoptosis and pyroptosis in cancer. *Cell Death Discov* 2020;6:112.
22 Cao X, Fu M, Bi R, *et al*. Cadmium induced BEAS-2B cells apoptosis and mitochondria damage via MAPK signaling pathway. *Chemosphere* 2021;263.
23 Ren Q, Guo F, Tao S, *et al*. Flavonoid fisetin alleviates kidney inflammation and apoptosis via inhibiting SRC-mediated NF-KB P65 and MAPK signaling pathways in septic AKI mice. *Biomed Pharmacother* 2020;122:109772.
24 Yap TA, Parkes EE, Peng W, *et al*. Development of immunotherapy combination strategies in cancer. *Cancer Discov* 2021;11:1368–97.
25 Zi M, Xingyu C, Yang C, *et al*. Improved antitumor immunity of chemotherapy in OSCC treatment by gasdermin-E mediated pyroptosis. *Apoptosis* 2023;28:348–61.
26 Kim MS, Chang X, Yamashita K, *et al*. Aberrant promoter methylation and tumor suppressive activity of the Dfna5 gene in colorectal carcinoma. *Oncogene* 2008;27:3624–34.
27 Fan J-X, Deng R-H, Wang H, *et al*. Epigenetics-based tumor cells pyroptosis for enhancing the immunological effect of chemotherapeutic nanocarriers. *Nano Lett* 2019;19:8049–58.
28 Wang M, Wu M, Liu X, *et al*. Pyroptosis remodeling tumor microenvironment to enhance pancreatic cancer Immunotherapy driven by membrane anchoring photosensitizer. *Adv Sci (Weinh)* 2022;9:2202914.
29 Zhang D, Man D, Lu J, *et al*. Mitochondrial TSPO promotes hepatocellular carcinoma progression through ferroptosis inhibition and immune evasion. *Adv Sci (Weinh)* 2023;10:2206669.
30 Mishchenko T, Balalaeva I, Gorokhova A, *et al*. Which cell death modality wins the contest for photodynamic therapy of cancer *Cell Death Dis* 2022;13:455.
31 Wang R, Li X, Yoon J. Organelle-targeted photosensitizers for precision photodynamic therapy. *ACS Appl Mater Interfaces* 2021;13:19543–71.
32 Wang H, Jing G, Niu J, *et al*. A mitochondria-anchored supramolecular photosensitizer as a pyroptosis inducer for potent photodynamic therapy and enhanced antitumor immunity. *J Nanobiotechnol* 2022;20:513.
33 Zeng S, Chen C, Zhang L, *et al*. Activation of pyroptosis by specific organelle-targeting photodynamic therapy to amplify immunogenic cell death for anti-tumor immunotherapy. *Bioact Mater* 2023;25:580–93.
34 Zhang X, Han J, Xu Y, *et al*. TSPO deficiency exacerbates GSDMD-mediated macrophage pyroptosis in inflammatory bowel disease. *Cells* 2022;11:856.
35 Zhong Y-T, Cen Y, Xu L, *et al*. Recent progress in carrier-free nanomedicine for tumor phototherapy. *Adv Healthc Mater* 2023;12:e2202307.
36 Qiu Y, Shi Y-N, Zhu N, *et al*. A lipid perspective on regulated pyroptosis. *Int J Biol Sci* 2023;19:2333–48.
37 Stefani C, Miricescu D, Stanescu-Spinu I-I, *et al*. Growth factors, PI3K/AKT/mTOR and MAPK signaling pathways in colorectal cancer pathogenesis: where are we now. *Int J Mol Sci* 2021;22:10260.
38 García-Hernández L, García-Ortega MB, Ruiz-Alcalá G, *et al*. The P38 MAPK components and modulators as biomarkers and molecular targets in cancer. *Int J Mol Sci* 2021;23:370.
39 Al Zein M, Boukhdoud M, Shammaa H, *et al*. Immunotherapy and immunoevasion of colorectal cancer. *Drug Discov Today* 2023;28:103669.
40 San-Román-Gil M, Torres-Jiménez J, Pozas J, *et al*. Current landscape and potential challenges of immune checkpoint inhibitors in microsatellite stable metastatic colorectal carcinoma. *Cancers (Basel)* 2023;15:863.
41 Baraibar I, Mirallas O, Saoudi N, *et al*. Combined treatment with immunotherapy-based strategies for MSS metastatic colorectal cancer. *Cancers (Basel)* 2021;13:6311.
42 Hsu S-K, Li C-Y, Lin I-L, *et al*. Inflammation-related pyroptosis, a novel programmed cell death pathway, and its crosstalk with immune therapy in cancer treatment. *Theranostics* 2021;11:8813–35.
43 Wu J, Wang L, Xu J. The role of pyroptosis in modulating the tumor immune microenvironment. *Biomark Res* 2022;10:45.
44 Yu P, Zhang X, Liu N, *et al*. Pyroptosis: mechanisms and diseases. *Signal Transduct Target Ther* 2021;6:128.
45 Huang C, Li J, Zhang C. What role does pyroptosis play in cancer? *Mol Metab* 2022;65:101587.
46 Xu M, Song B, Yang X, *et al*. The combination of decitabine and aspirin inhibits tumor growth and metastasis in non-small cell lung cancer. *J Int Med Res* 2022;50:030006052211120.
47 Zhu Z, Lin S, Wu X, *et al*. Decitabine and cisplatin are synergistic to exert anti-tumor effect on gastric cancer via inducing Sox2 DNA demethylation. *Onco Targets Ther* 2021;14:623–36.
48 Li X, Li Y, Dong L, *et al*. Decitabine priming increases anti-PD-1 antitumor efficacy by promoting CD8+ progenitor exhausted T cell expansion in tumor models. *J Clin Invest* 2023;133.
49 Wang Y, Tong C, Dai H, *et al*. Low-dose decitabine priming endows CAR T cells with enhanced and persistent antitumour potential via epigenetic reprogramming. *Nat Commun* 2021;12:409.
50 Yu G, Wu Y, Wang W, *et al*. Low-dose decitabine enhances the effect of PD-1 blockade in colorectal cancer with microsatellite stability by re-modulating the tumor microenvironment. *Cell Mol Immunol* 2019;16:401–9.